DEFLUORINATION

Low-temperature mineralization of perfluorocarboxylic acids

Brittany Trang[1]†, Yuli Li[2,3]†, Xiao-Song Xue[4], Mohamed Ateia[1]‡, K. N. Houk[3]*, William R. Dichtel[1]*

Per- and polyfluoroalkyl substances (PFAS) are persistent, bioaccumulative pollutants found in water resources at concentrations harmful to human health. Whereas current PFAS destruction strategies use nonselective destruction mechanisms, we found that perfluoroalkyl carboxylic acids (PFCAs) could be mineralized through a sodium hydroxide–mediated defluorination pathway. PFCA decarboxylation in polar aprotic solvents produced reactive perfluoroalkyl ion intermediates that degraded to fluoride ions (78 to ~100%) within 24 hours. The carbon-containing intermediates and products were inconsistent with oft-proposed one-carbon-chain shortening mechanisms, and we instead computationally identified pathways consistent with many experiments. Degradation was also observed for branched perfluoroalkyl ether carboxylic acids and might be extended to degrade other PFAS classes as methods to activate their polar headgroups are identified.

Per- and polyfluoroalkyl substances (PFAS) are anthropogenic substances containing multiple C–F bonds. PFAS are used as omniphobic surfactants in many industrial processes and products, including in poly(tetrafluoroethylene) production; as water-, oil-, and stain-resistant barriers for fabrics and food service containers; and as components of aqueous film–forming foams for fire suppression (*1*). As a result of their widespread global use, environmental persistence, and bioaccumulation, PFAS contamination is pervasive (*2*) and affects drinking water, surface waters, livestock, and agricultural products around the world (*3*). This persistent environmental contamination is alarming because chronic exposure to even low levels of these compounds is associated with negative health effects such as thyroid disease, liver damage, high cholesterol, reduced immune responses, low birth weights, and several cancers (*4*). Many of these effects have been obscured by PFAS manufacturers for decades (*5*). The growing focus on removing parts-per-billion to parts-per-trillion levels of PFAS contamination from drinking water supplies has produced several PFAS-removal approaches, including established adsorbents such as activated carbon and ion-exchange resins, as well as emerging materials such as cross-linked polymers (*6*, *7*). Adsorbents or membrane-based separation processes create PFAS-contaminated solid or liquid waste streams but do not address how to degrade these persistent pollutants. PFAS destruction is a daunting task because the strong C–F bonds that give PFAS their desirable properties also make these compounds resistant to end-of-life degradation. Harsh PFAS degradation methods include incineration (*8*), ultrasonication (*9*, *10*), plasma-based oxidation (*11*), electrochemical degradation (*12*, *13*), supercritical water oxidation (*14*), ultraviolet-initiated degradation using additives such as sulfite or iron (*15*–*19*), and other combinations of chemical and energy inputs (*20*) (table S1). Leveraging the reactivity of perfluoroalkyl species might, however, offer milder alternatives to address the PFAS contamination problem.

The opportunity to degrade PFAS at high concentrations in nonaqueous solvents has recently been developed using PFAS adsorbents that can be regenerated using a simple solvent wash. This development enables the destruction of these compounds after they have been removed from water resources, which broadens suitable degradation conditions beyond dilute aqueous environments. Here, we accessed reactive perfluoroalkyl anions that are mineralized under mild conditions by decarboxylating perfluorocarboxylic acids (PFCAs), one of the largest classes of PFAS compounds, at low temperatures in dipolar aprotic solvents (Fig. 1). PFCAs of various chain lengths undergo efficient mineralization in the presence of NaOH in mixtures of water and dimethyl sulfoxide (DMSO) at mild temperatures (80 to 120°C) and ambient pressure. Under these conditions, perfluorooctanoic acid (PFOA, **1**) is completely degraded with >90% defluorination and minimal formation of fluorocarbon by-products. Experimental observations and density functional theory (DFT) calculations offer strong evidence for degradation pathways distinct from the single-carbon-chain shortening processes proposed in prior PFAS degradation studies (*11*, *16*, *18*, *21*–*23*). This reactivity mode is immediately promising for PFCA destruction and may prove generalizable to other PFAS classes as methods to activate their polar groups are identified.

[1]Department of Chemistry, Northwestern University, Evanston, IL 60208, USA. [2]Department of Chemistry, School of Science, Tianjin University, Tianjin 300354, China. [3]Department of Chemistry and Biochemistry, University of California, Los Angeles, Los Angeles, CA 90095, USA. [4]Key Laboratory of Organofluorine Chemistry, Shanghai Institute of Organic Chemistry, University of Chinese Academy of Sciences, Chinese Academy of Sciences, Shanghai 200032, P.R. China.
*Corresponding author. Email: houk@chem.ucla.edu (K.N.H.); wdichtel@northwestern.edu (W.R.D.)
†These authors contributed equally to this work.
‡Present address: Center for Environmental Solutions & Emergency Response, US Environmental Protection Agency, Cincinnati, OH, USA.

Decarboxylation and defluorination of PFCAs in polar aprotic solvent

Perfluoroalkylcarbanions are easily accessed by decarboxylating PFCAs in dipolar aprotic solvents. In a solution of DMSO and H_2O (8:1 v/v) at 120°C, PFOA decarboxylates to form perfluoro-1H-heptane **2**, which phase separates from solution as an oil. ^{1}H, ^{13}C, and ^{19}F nuclear magnetic resonance (NMR) spectroscopy of the isolated oil confirmed the formation of the decarboxylated product in high purity (figs. S1 to S4). This decarboxylation reaction is consistent with those reported by Kong *et al.*, who found that most carboxylic acids decarboxylate reversibly in dimethylformamide (*24*). Zhou *et al.* (*25*) studied the origins of this reversible carboxylation computationally and determined that the lower barrier to decarboxylation was fully induced by solvent effects from the polar aprotic solvent (figs. S45 and S58). Such reactivity has also been observed as a complication for analytical standards (*26*, *27*). We found that when the same PFOA solution in DMSO/H_2O was subjected to the decarboxylation conditions but in the presence of NaOH (30 equiv), PFOA instead degraded to a mixture of fluoride, trifluoroacetate ions, and carbon-containing by-products (Fig. 2A). Degradation also occurred in other polar aprotic solvents such as dimethylacetamide and sulfolane but did not proceed in pure water (fig. S20 and table S3). ^{19}F NMR spectroscopy of reaction aliquots collected over 24 hours indicated that resonances corresponding to PFOA were no longer detectable within 14 hours. Unexpectedly, no resonances corresponding to perfluoroalkyl groups containing between four and seven carbons were observed. Resonances corresponding to sodium perfluoropropionate ($CF_3CF_2CO_2Na$) at –81.5 and –118.2 ppm were observed just above the baseline within spectra of aliquots collected at reaction times shorter than 24 hours but were absent in spectra of later aliquots (fig. S10). The only prominent fluorine resonance in the aliquot sampled at 24 hours corresponds to sodium trifluoroacetate (CF_3CO_2Na, –73.6 ppm; Fig. 2B). Integration of this resonance indicated that its intensity plateaued at ~4 to 24 hours, corresponding to only 7% of the F content and 9% of the C content relative to the initial PFOA concentration (Fig. 2, A and C). The resonance from CF_3CO_2Na ions eventually decreased in intensity and presumably degraded into fluoride, albeit much more slowly than the rate of PFOA disappearance (Fig. 2C, inset). This resonance disappeared over 300 hours, which we confirmed

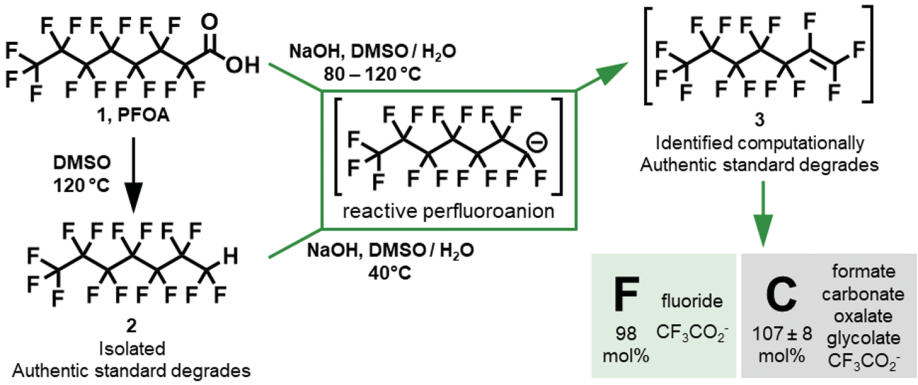

Fig. 1. Overview of degradation pathways identified in this study. Heating PFCAs in polar aprotic solvents such as DMSO decarboxylates them to 1H-perfluoroalkanes. When this reaction was performed in the presence of NaOH, the PFCA mineralized to fluoride, sodium trifluoroacetate, and nonfluorinated carbon-containing products. The 1H-perfluoroalkane underwent the same degradation process at even lower temperatures. Computational studies identified the corresponding perfluoroalkenes as likely intermediates, and an authentic standard of the seven-carbon perfluoroalkene was competent for the degradation.

by subjecting an authentic sample of sodium trifluoroacetate to the same reaction conditions (fig. S24). PFOA degradation is thus rapid and forms CF_3CO_2Na and trace $CF_3CF_2CO_2Na$ as the only identifiable perfluoroalkyl-containing liquid-phase by-products, each of which continues to degrade over extended reaction times. Subjecting perfluorooctane sulfonate ions to the basic decarboxylation conditions did not result in decreasing perfluoroalkyl ^{19}F NMR integrations or fluoride formation (fig. S19 and table S3), indicating that decarboxylation to the reactive anion intermediate is the key first step of the defluorination process for PFCAs.

Ion chromatography (IC) indicated that 90 ± 6% of the fluorine atoms originating from the PFOA were recovered as fluoride ions after 24 hours of reaction at 120°C (fig. S29). Control experiments showed that the fluorinated polytetrafluoroethylene reaction vessels did not contribute an appreciable amount of fluoride to fluoride recovery (table S3). Fluoride analyses performed by IC at shorter reaction times indicated that fluoride increased proportionally to the decrease in [PFOA] observed by ^{19}F NMR spectroscopy. This high fluoride recovery indicates that most of the perfluoroalkyl fluorines were defluorinated and mineralized rather than being transformed to smaller-chain PFAS or being lost as volatile fluorocarbons.

Degradation of varied PFAS and by-product analysis suggest a complex mechanism

PFCAs with different chain lengths (two to nine carbons) were degraded, providing fluoride recoveries between 78% and quantitative at 24 hours for all PFCAs with four or more carbons (Fig. 2D). Although the longer-chain (C ≥ 4) PFCAs had a degradation profile similar to that of PFOA in that their perfluoroalkyl peaks disappeared from the ^{19}F NMR spectra (fig. S22) and $CF_3CO_2^-$ was formed (Fig. 2D and fig. S23), the destruction of shorter-chain PFCAs (C = 2, 3) was slower and appeared to occur by different mechanisms. For trifluoroacetate (C = 2), degradation is slow (>6 days; fig. S24), likely because the instability of the CF_3^- anion (*28*) hinders decarboxylation, such that destruction occurs either more slowly or by a different mechanism. The carbanion corresponding to perfluoropropionic acid (PFPrA) (C = 3) decarboxylation is similarly unstable (*28*), resulting in degradation faster than trifluoroacetate but slower than the longer PFCAs (fig. S22). Although the PFPrA ^{19}F NMR peaks disappeared completely over 3 days, fluoride recovery was lower than in other PFCAs (3.9 ± 1.6%; Fig. 2D). PFPrA, unlike others in the series, decarboxylates to form a volatile product; in the ^{19}F NMR for PFPrA degradation, peaks corresponding to CF_3CF_2H can be identified (figs. S11 and S12). Headspace gas chromatography–electron-impact mass spectrometry (MS) also detected the $CF_3CF_2^{+\bullet}$ fragment in the gas phase of the reaction (fig. S40). This finding was corroborated by atmospheric pressure chemical ionization–MS of a liquid aliquot of the reaction that had a prominent peak corresponding to $CF_3CF_2^-$ (compare fig. S39 with figs. S38 and S40). It appears to be more favorable to produce volatile CF_3CF_2H than for the C = 3 PFCA to proceed down the destruction pathway; as discussed below, this supports our proposal that a γ-carbon is necessary for the major defluorination pathway to occur. Previous PFAS degradation studies have suggested that PFCAs (or other PFAS that are PFCA precursors) degrade through a decarboxylation-hydroxylation-elimination-hydrolysis (DHEH) pathway in which each PFCA is shortened by one carbon each cycle, producing successively shorter PFCAs (*11*, *16*, *18*, *21*–*23*). However, the nonconformal degradation of the three-carbon acid and the products observed in the ^{19}F NMR spectra of degradation reactions of PFCAs containing four or more carbons in the present study indicated that degradation instead occurs through distinct, non-single-carbon shortening mechanisms under these conditions.

The hypothesis that degradation does not occur by iterative one-carbon shortening was further supported by quantifying the carbon-containing by-products formed when PFOA was degraded for 24 hours. We examined a combination of solution ^1H and ^{19}F NMR spectroscopy and quantitative ^{13}C NMR spectroscopy of the precipitate isolated from the reaction and dissolved in D_2O. We also performed ion chromatography on the combined solution and precipitate by adding water to the reaction mixture until the precipitate redissolved. These measurements accounted for the complete carbon balance of the PFOA degradation (107 ± 8 mol% C relative to the $[PFOA]_0$; table S4 and fig. S30). Other than the residual $CF_3CO_2^-$ ions described above, which continued to degrade at longer reaction times, no other organofluorine compounds were detected. Instead, one-, two-, and three-carbon products lacking C–F bonds were identified and quantified. Formate ions were found in solution (fig. S9) and in the precipitate, corresponding to 2.5 ± 0.3 mols formate ions/mol PFOA, as determined by combining the formate concentrations measured in the solution and precipitate by NMR spectroscopy. This amount is consistent with ion chromatography of the reaction mixture and redissolved precipitate, which provided 2.1 ± 0.2 mols formate/mol PFOA. Formate formation and the varying amounts of formate produced by PFCAs of other chain lengths inspired a deeper mechanistic study (see below). Carbonate ions were detected exclusively in the precipitate, corresponding to 2.1 ± 0.3 mols/mol PFOA. The most likely source of carbonate ions was from the initial decarboxylation step, along with other downstream processes that generate carbon dioxide or single-carbon products at the same oxidation state. Two-carbon products, glycolate ions (0.6 ± 0.1 mol/mol PFOA) and oxalate ions (0.7 ± 0.1 mol/mol PFOA), were found in the precipitate, along with three-carbon-containing tartronate ions (0.2 ± 0.1 mol/mol PFOA). The glycolate and oxalate ions were identified by ^{13}C NMR spectroscopy and comparison with authentic standards. Tartronate ions were identified by a combination of ^{13}C and ^1H NMR spectroscopy, which were consistent with literature reports (*29*) and showed the expected correlations in two-dimensional NMR experiments (figs. S31 and S32). Finally, a small amount of the PFOA carbon balance was found in an unknown product, which

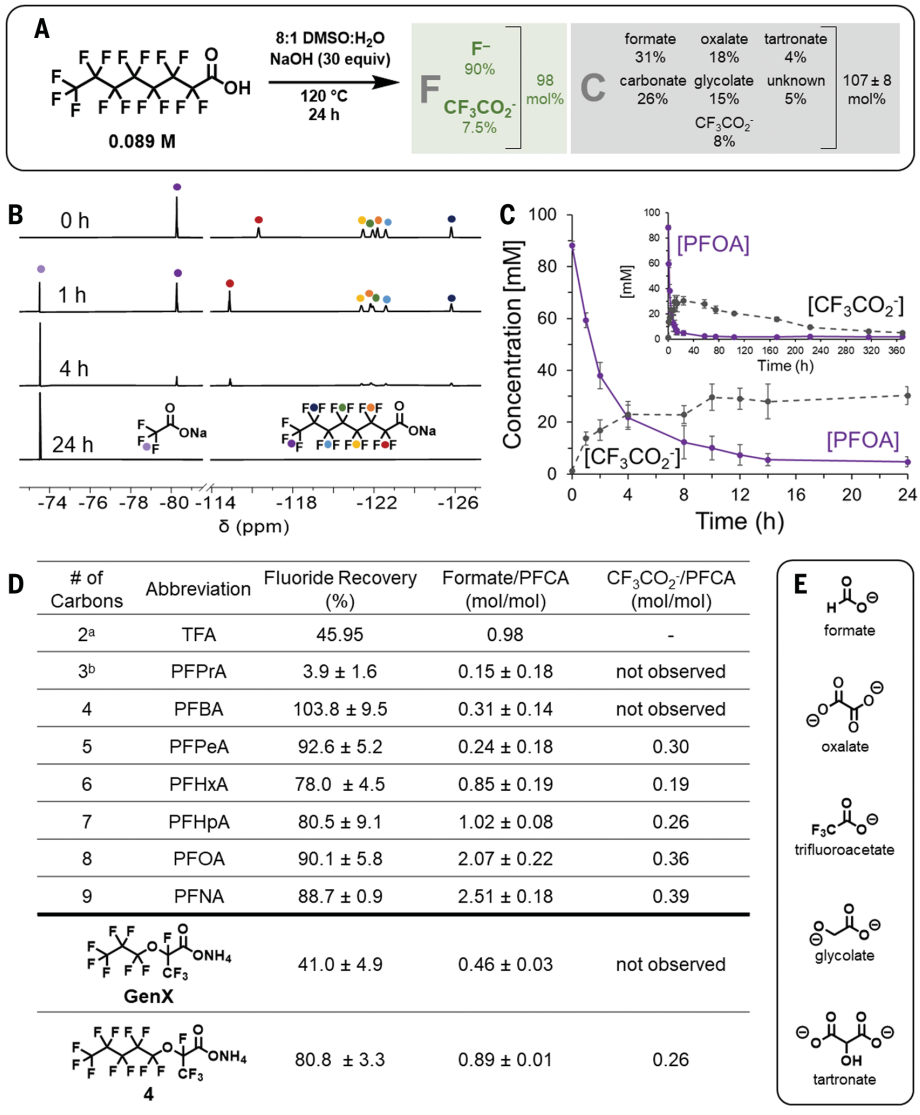

Fig. 2. Overall reaction scheme, experiments monitoring PFOA and $CF_3CO_2^-$ concentrations over the course of the reaction, and summary of degradation products from a series of PFCAs of different lengths. (**A**) Heating 0.089 M PFOA in 8:1 DMSO:H_2O with 30 equiv NaOH allowed 90% of the initial fluorine to be recovered as inorganic fluoride and residual trifluoroacetate with few other organofluorine by-products. Formate ions (26 mol %) and several other nonfluorinated by-products were identified (107 ± 8 mol %). (**B**) ^{19}F NMR spectra from 0 to 24 hours. Peaks corresponding to PFOA perfluoroalkyl fluorines between −115 and −126 ppm, as well as at −80 ppm, disappeared in less than 24 hours. Trifluoroacetate (−73.6 ppm) appeared and disappeared (disappearance shown in inset of panel C) more slowly over the course of the reaction. (**C**) Amount of PFOA (purple, solid line) and sodium trifluoroacetate (gray, dashed line) in the reaction over time. Error bars correspond to the standard deviation of three experiments. (**D**) Fluoride recovery was calculated as mols fluoride after reaction as detected by ion chromatography per mol fluorine in PFCA reactant. Formate/PFCA was calculated as mols formate as detected by IC after reaction per mol PFCA reactant. $CF_3CO_2^-$/PFCA was determined as mols $CF_3CO_2^-$ as calculated from ^{19}F NMR spectroscopy after 24 hours of reaction per mol PFCA reactant. All measurements are expressed as the average of three trials unless specified otherwise, and error is expressed as a standard deviation. All reaction times are 24 hours unless specified otherwise. "a," 286 hours, single measurement; "b," 63% ± 12% of PFPrA starting material degraded after 24 hours. (**E**) Structures of the identified carbon-containing by-products.

# of Carbons	Abbreviation	Fluoride Recovery (%)	Formate/PFCA (mol/mol)	$CF_3CO_2^-$/PFCA (mol/mol)
2[a]	TFA	45.95	0.98	-
3[b]	PFPrA	3.9 ± 1.6	0.15 ± 0.18	not observed
4	PFBA	103.8 ± 9.5	0.31 ± 0.14	not observed
5	PFPeA	92.6 ± 5.2	0.24 ± 0.18	0.30
6	PFHxA	78.0 ± 4.5	0.85 ± 0.19	0.19
7	PFHpA	80.5 ± 9.1	1.02 ± 0.08	0.26
8	PFOA	90.1 ± 5.8	2.07 ± 0.22	0.36
9	PFNA	88.7 ± 0.9	2.51 ± 0.18	0.39
GenX		41.0 ± 4.9	0.46 ± 0.03	not observed
4		80.8 ± 3.3	0.89 ± 0.01	0.26

we designated as a secondary degradation product derived from the reaction of glycolate ions with other intermediates because it was formed in greater amounts when glycolic acid was included at the beginning of the PFOA degradation reaction. Identifying and quantifying these carbon products has important implications for PFOA degradation. First, the high recovery of products with no C–F bonds, along with the high fluoride ion recovery, confirms that these conditions efficiently mineralize PFCAs. Furthermore, identifying multiple two- and three-carbon by-products further implicates mechanisms more complicated than iterative one-carbon shortening processes.

PFCAs of different lengths degraded by different pathways, as indicated by the distinct patterns in their formate and $CF_3CO_2^-$ formation. If the chain-shortening DHEH mechanism were operative, then we would expect that resonances belonging to chain-shortened species would appear transiently in the ^{19}F NMR spectra as longer-chain PFCAs speciated into a distribution of shorter-chain PFCAs. Instead, only ^{19}F NMR peaks corresponding to $CF_3CO_2^-$ and trace amounts of $CF_3CF_2CO_2^-$ were detected, and the following by-product patterns emerged. PFCAs containing four or fewer carbons did not produce any $CF_3CO_2^-$, but all PFCAs containing more than four carbons produced roughly the same substoichiometric amount of $CF_3CO_2^-$: ~0.3 equivalents of $CF_3CO_2^-$/mol PFCA. PFCAs containing fewer than six carbons did not produce substantial amounts of formate (Fig. 2D), but PFCAs containing six or more carbons produced increasing amounts of formate, with C = 6 and 7 producing ~1 equivalent of formate per PFCA, C = 8 ~2 equivalents, and C = 9 ~2.5 equivalents. These observations indicate that $CF_3CO_2^-$ and formate production occur by distinct pathways.

Experiments conducted at near-ambient temperatures showed that decarboxylation is the rate-limiting step and subsequent defluorination and chain-shortening steps can occur at near-ambient temperature, giving experimental insight into the possible mechanism. Substantial defluorination still occurred when the isolated PFOA degradation product (perfluoro-1H-heptane **2**) was subjected to degradation conditions but heated to only 40°C (table S3). PFCAs have historically been decarboxylated by heating PFCA salts in ethylene glycol at 190 to 230°C to yield perfluoro-1H-alkanes (*30*) or by pyrolyzing PFCA salts at 210 to 300°C to yield perfluoro-1-alkenes (*31*), but dipolar aprotic solvent-assisted degradation enabled decarboxylation at only 80 to 120°C, which can be followed by an even lower-temperature defluorination. When **2** was subjected to the basic degradation conditions, both fluoride and chain-shortened PFCAs were observed by IC and ^{19}F NMR at short reaction times (5 min at 120°C) and low temperatures (25 min at 40°C), in contrast to

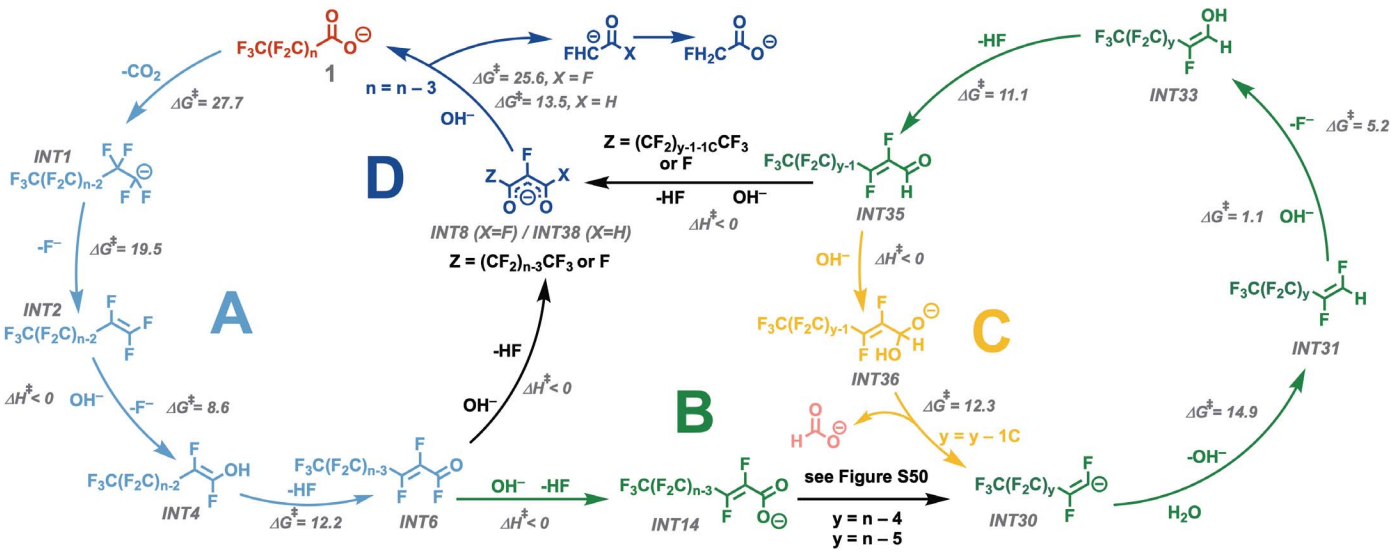

Fig. 3. Proposed PFCA degradation mechanism with activation energies (ΔG‡, kcal/mol) for each step as calculated at the M06-2X/6-311+G(2d,p)-SMD(DMSO) level. Cycle AD shows a three-carbon shortening of the original PFCA of *n* carbons ("1," red, top) with one carbon lost as CO_2 (converted to CO_3^{2-} under basic conditions) and two carbons lost to fluoroacetic acid, which readily degrades under these reaction conditions. Pathway B shows the reaction that results from the 1,2 addition of hydroxide to the carboxyl carbon of INT6. Proposed pathways for the conversion of INT14 to INT30, along with pathways for nonfluorinated, carbon-containing by-products, are described in fig. S50. The alkene INT30 becomes protonated and proceeds through a similar pathway as pathway A. At INT35, the aldehyde analog of acid fluoride INT6, 1,2 addition to the carboxyl carbon leads to the formation of formate by elimination in pathway C, whereas 1,4 addition to the β carbon leads back to pathway D. All energies are expressed in units of kilocalories per mole.

reactions starting from the carboxylated PFOA at the same conditions, in which no fluoride or short-chain PFCAs were formed at short reaction times or at low temperatures (table S3). Degradation of **2** at 40°C for 48 hours showed 57% defluorination (table S3). Although the insolubility of the polyfluoroalkane standard in the DMSO and water solvent precluded accurate measurements of its concentration by NMR spectroscopy, the presence of the $CF_3CO_2^-$ ^{19}F NMR peak (fig. S13) indicated that the decarboxylated material likely followed a similar degradation pathway. In this low-temperature experiment, intermediates that were not observed in the higher-temperature experiments became evident; at around –210 ppm, a triplet with J = 48 Hz appeared, which corresponds to the fluoroacetate ion (CH_2FCOO^-; fig. S13). The fluoroacetate peak did not appear in the higher-temperature degradations because it degrades rapidly at those temperatures, as confirmed by the degradation of a pure standard. Temperature-dependent studies of the original PFOA degradation reaction showed that the reaction slowed slightly when the reaction was conducted at 100°C (time to [PFOA] = 0 is ~100 hours compared with 16 hours for 120°C; figs. S21 and S25 to S27) and slowed substantially when lowered to 80°C (>290 hours; figs. S21 and S28). Therefore, significant defluorination of **2** was unexpected at 40°C, suggesting that the steps after the decarboxylation were low-barrier or barrierless. These observations further indicate that degradation does not proceed by successive chain shortening through iterative decarboxylation steps.

Computational studies reveal steps in defluorination mechanism with negligible barriers

DFT was used to determine the mechanism of this degradation reaction. These studies predicted that decarboxylation is the rate-limiting step of the degradation and that a series of low-barrier or enthalpically barrierless reactions can lead to levels of defluorination consistent with experimental observations. DFT calculations were performed at the M06-2X/6-311+G(2d,p)-SMD(DMSO) level (see the supplementary materials for details) and used PFOA as the starting point for the calculations. This mechanism should also be valid for the degradation of straight-chain PFCAs of other lengths. After the initial decarboxylation of PFOA (compound **1**; Fig. 3) at an activation energy of about 28 kcal/mol, calculations indicated that the resulting anion INT1 would eliminate a fluoride to become perfluoroalkene INT2 (Fig. 3 and fig. S44). Unlike previous PFCA degradation mechanisms in the literature predicting that the perfluoroalkyl fragment will hydroxylate after decarboxylation (*11*, *16*, *18*, *21*–*23*), these computational results point to the formation of an alkene followed by an enthalpically barrierless hydroxylation of the activated electrophilic alkene. Hydroxylation of the alkyl fragment INT1, as postulated in previous studies, was calculated to have an activation energy of 29.7 kcal/mol under our study's conditions after protonation of the fragment (fig. S46), whereas formation of the alkene INT2 had a barrier of 19.5 kcal/mol, followed by a hydroxylation with no enthalpic barrier (ΔG = –44.3 kcal/mol). The highly exothermic nature of this alkene hydroxylation step played a leading role in driving the degradation, consistent with observations that the defluorination and chain-shortening steps of the reaction neither have high energy barriers nor lead to the formation of successively shorter PFCAs. Accordingly, when perfluoro-1-heptene **3** (INT2) was subjected to degradation conditions (table S3), it also degraded to similar products even at 40°C, corroborating the computational prediction and indicating that the alkene is likely on the degradation pathway. Further, calculations also suggested that the hydroxylation is specifically favored at the terminal position, because addition on the internal side of the alkene had a barrier of 8.9 kcal/mol (fig. S47). After this alkene hydroxylation (INT4), calculations suggested that a series of low- or no-barrier reactions occurred, as shown in Fig. 3 and fig. S44. The enol can then eliminate another fluoride, forming α,β-unsaturated acyl fluoride INT6 through retro 1,4-conjugate addition.

This resulting α,β-unsaturated acid fluoride INT6 has two plausible reaction pathways that are consistent with the experimental findings: a 1,4-conjugate addition that leads to $CF_3CO_2^-$ formation (pathway D) or a 1,2 addition (pathway B) that can lead to formate formation (pathway C), which together explain

the experimentally observed by-product distribution. Calculations indicated that neither option had enthalpic barriers and thus very low free energies of activation, indicating that both reactions occurred to some extent (fig. S48). In the enthalpically barrierless 1,4-conjugate addition (Fig. 3, pathway D, X = F) that leads to the formation of shorter PFCAs such as $CF_3CO_2^-$, the hydroxide adds to the β carbon of α,β-unsaturated acyl fluoride INT6, followed by an enthalpically barrierless fluoride elimination to form 1,3-diketone compound INT8. Hydroxide again adds to this intermediate on the ketone carbonyl side to generate INT9, which is more favorable than the addition on the acyl fluoride side (fig. S49). Finally, fragmentation occurs to generate an equivalent of PFCA three carbons shorter than the initial carboxylic acid and an equivalent of fluoroacetic acid, which was observed in the experiments conducted at 40°C (figs. S13 and S16). As an example, if five-carbon PFCA perfluoropentanoic acid (PFPeA) went through this cycle, it would produce an equivalent of carbon dioxide (1 carbon), an equivalent of trifluoroacetic acid (2 carbons), and an equivalent of fluoroacetic acid (2 carbons) by this pathway. However, from the experimental results, only about 0.3 equiv of $CF_3CO_2^-$ were produced from PFPeA (Fig. 2D), indicating the PFCA degradation does not proceed quantitatively by this process. This pathway also does not account for the substantial amounts of formate produced in reactions from longer PFCAs.

Formate ion production is explained by a pathway stemming from the favorable 1,2-hydroxylation product, which provides an α,β-unsaturated PFCA (pathway B). As with INT6, there are multiple possible sites for hydroxide addition to INT14, either to the α (13.6 kcal/mol) or β (12.0 kcal/mol) carbons. Possible pathways propagating from both of these processes, along with the formation of oxalate and other carbon by-products, are described in the supplementary materials (figs. S50 to S54). Although both of these pathways for the conversion of INT14 to INT30 are plausible and supported by computation, the possibility of other active mechanisms cannot be ruled out. However, both of these hydroxylations are more favorable than decarboxylating the α,β-unsaturated perfluoroacid (22.3 kcal/mol), and both lead to the formation of perfluoroalkene anion INT30. The chain length of the alkene depends on which hydroxylation pathway the substrate follows, either four carbons shorter than the original chain (1,3 addition) or five carbons shorter than the original chain (1,4 addition). Calculations showed that perfluoroalkene anion INT30 is protonated rather than eliminating a fluoride to generate the alkyne (figs. S55 and S56). After the protonation, hydroxide adds to the alkene, much like the first postdecarboxylation step in the first proposed pathway. Likewise, α,β-unsaturated aldehyde INT35, an analog to the α,β-unsaturated acid fluoride INT6, is generated through retro-1,4 addition. At this point, the intermediate again faces a bifurcation, with opportunities for both the 1,4-conjugate addition and the 1,2 addition of the hydroxide to the α,β-unsaturated aldehyde. Similar to the addition to the α,β-unsaturated acyl fluoride, both of these reactions were calculated to have no enthalpic barrier (fig. S57). Through the 1,4-conjugate addition (Fig. 3, pathway D, X = H; figs. S59 and S60), the 1,3-diketone compound generated will be attacked by hydroxide, followed by the same fragmentation as noted before. That is, a PFCA and a fluoroacetic aldehyde are formed, the latter of which can be transformed into fluoroacetic acid or be rapidly hydrolyzed. However, if INT35 undergoes 1,2 addition of hydroxide to the α,β-unsaturated aldehyde (Fig. 3, pathway C; figs. S55 and S60), the resulting aldehyde (INT36) cannot eliminate a hydride, whereas its acid fluoride counterpart INT13 can eliminate a fluoride. Instead, INT36 can eliminate the entire perfluoroalkyl chain, creating an equivalent of formate and a one-carbon-shorter alkene anion that can either exit the cycle through 1,4-conjugate addition or proceed through the cycle again to form more formate, thus giving rise to the trend of increased formate formation by PFCAs of longer chain length.

Experimental support for the computationally determined mechanism

Our calculations affirmed that decarboxylation is the rate-determining step of the degradation, and the calculated activation energy of ~28 kcal/mol is consistent with the experimentally determined value of 30.0 kcal/mol (see the supplementary materials, page 6 and table S2). The proposed mechanism is also supported by experimental observations of $CF_3CO_2^-$ and the formate distribution shown in Fig. 2D. By this mechanism, $CF_3CO_2^-$ was produced as a nonstoichiometric by-product, in accordance with the observation that only ~0.3 to 0.4 equivalents of $CF_3CO_2^-$ were formed per mol PFCA for all PFCAs with C ≥ 5. This proposed mechanism also explains why four-carbon perfluorobutanoic acid (PFBA) did not produce $CF_3CO_2^-$, whereas the five-carbon PFPeA did, because PFBA that has gone through cycle AD would create $FCOO^-$, which will decompose spontaneously to carbon dioxide and fluoride (*32*) or hydrolyze from INT8 to form tartronate. This two-cycle mechanism also explains why five-carbon PFPeA produced $CF_3CO_2^-$ but no formate, because the carbon chain is not long enough to go through pathway C. The mechanism predicts that the amount of formate will increase as the length of the initial PFCA carbon chain increases; this was also affirmed by experimental results for PFCAs of six to nine carbons (Fig. 2D). The formation of carbonaceous by-products such as oxalate, glycolate, and tartronate is also consistent with this mechanism (figs. S50 to S54). Furthermore, when conducting reactions with protodecarboxylated perfluoro-1H-heptane **2** or perfluoro-1H-hexane **S1** (figs. S5 to S8) at 40°C, the formation of intermediate products containing five- or four-carbon fluorous chains was observed (figs. S14 and S17), respectively, which likely correspond to INT8/INT9 (figs. S15 and S18), the intermediate with the highest activation energy (25.6 kcal/mol) in this pathway. The peaks corresponding to this intermediate disappeared as peaks corresponding to the five- and four-carbon PFCAs appeared. These PFCAs that are shortened by three carbons are the logical products of a single-pathway AD cycle from their respective starting materials. The experimental observations confirm that the computed mechanism provides a complete model to describe the observations made experimentally about this complex degradation. We also performed calculations to test proposed difluorocarbene (fig. S62), perfluoroalkyl hydroxylation (fig. S46), and α-lactone (*33*, *34*) (fig. S61) mechanisms that had been proposed for such degradations, but these were found to have barriers too high to be compatible with the experimental conditions.

Generalization of the PFCA destruction method to perfluoroalkyl ether carboxylates

Branched perfluoroalkyl ether carboxylic acids, another major class of PFAS contaminants, are also mineralized by perfluoroalkyl anion intermediates. The ammonium salt of hexafluoropropylene dimer acid (ammonium perfluoro (2-methyl-3-oxahexanoate; also known as FRD-902, the trade name GenX, or HFPO-DA in its acid form) is a perfluoroalkyl ether carboxylic acid that was introduced as an industrial replacement for PFOA. This compound now contaminates water sources such as the Cape Fear River, which serves as the primary drinking water source for >350,000 residents of North Carolina (*35*). For this compound, the decarboxylation and branched CF_3 chain defluorination occurred at 40°C, an even lower temperature than for the PFCAs (fig. S35). This finding is consistent with computational results indicating that the barrier for GenX decarboxylation is only 20.4 kcal/mol (fig. S63). However, because of the presence of the ether oxygen in place of the γ-carbon, the structure was unable to eliminate a γ-fluorine and instead formed perfluoroalkyl ether carboxylic acid intermediate ***5*** through hydrolysis (Fig. 4), which built up in solution and was observed by both ^{19}F NMR and electrospray ionization MS (figs. S33, S35, and S42). Further degradation occurred at elevated temperatures (80°C;

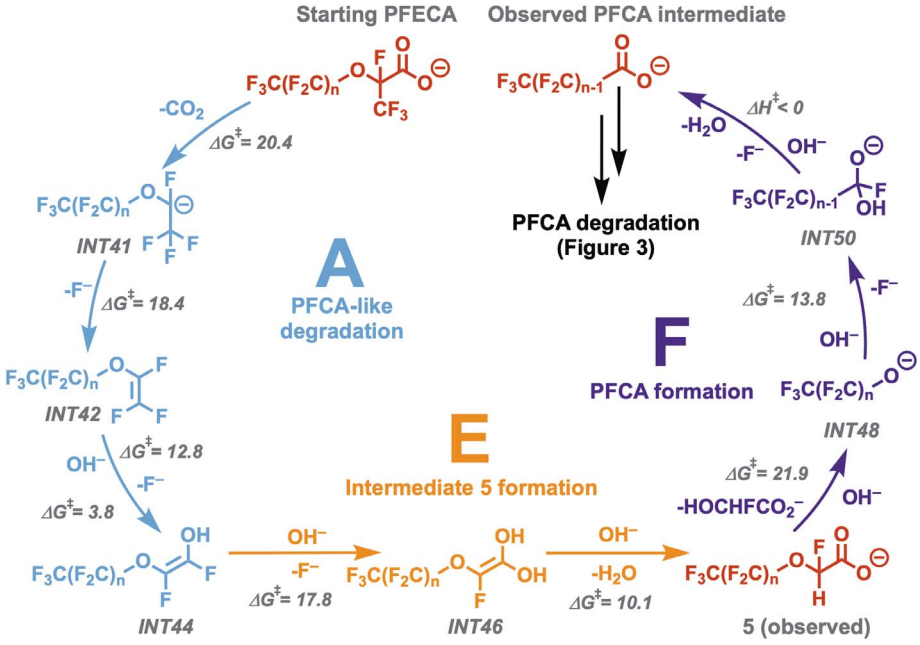

Fig. 4. Proposed mechanism for branched perfluoroalkyl ether carboxylic acid degradation. Pathway A (blue) shows the branched CF_3 defluorinating in the same manner as PFCAs in Fig. 3. The lack of γ-fluorines forces formation of **5** through pathway E (orange), as observed by NMR and MS. Calculations show the hydroxide-mediated S_N2 that eliminates the perfluoroalkoxide tail in pathway F (purple), leading to the formation of a PFCA that is degraded according to the mechanism described in Fig. 3. All energies are expressed in units of kilocalories per mole.

fig. S35). Calculations showed that the decarboxylation of this intermediate was unfavorable (figs. S65); rather, a hydroxide-mediated S_N2 with a barrier of 21.9 kcal/mol occurred in which the perfluoroalkoxide tail was eliminated (fig. S66). This perfluoroalkoxide formed a carboxylic acid ($\Delta G^{\ddagger}$ = 21.9 kcal/mol) with the same number of carbons as the original perfluoroether tail. Because GenX contains a three-carbon tail, it produced the C3 PFCA (PFPrA), the degradation of which led to incomplete defluorination (41%; Fig. 2D) and the formation of CF_3CF_2H (figs. S37, S40, and S41). These observations are consistent with those of the direct degradation of PFPrA (Fig. 2D and figs. S11, S12, S39, and S40). The experimental observations showed that temperatures of 40°, 80°, and 120°C are necessary to form intermediate **5**, to form the PFCA analog, and to initiate PFCA degradation, respectively. These temperature steps correspond to the calculated energy barriers of 20.4, 21.9, and 27.7 kcal/mol, respectively (figs. S35, S63, and S64). Degradation of a longer perfluoroalkyl ether carboxylic acid with a five-carbon perfluoroalkyl tail (compound **4**; figs. S34, S36, S40, and S43) proceeded by a similar mechanism as that of GenX and gave fluoride recoveries consistent with those obtained from the five-carbon PFCA PFPeA. These findings indicate that perfluoroalkyl ether carboxylates also degrade through perfluoroalkyl anion–based processes. Intermediates in the degradation of **4**, as observed by atmospheric pressure chemical ionization–MS (fig. S43), corroborated the proposed mechanism (Fig. 4).

Conclusions

The perfluorocarbon reactivity that we have described here leverages low-barrier defluorination mechanisms to mineralize PFAS at mild temperatures with high rates of defluorination and low organofluorine side-product formation. In contrast to other proposed PFAS degradation strategies, the conditions described here are specific to fluorocarbons, destroy concentrated PFCAs, give high fluoride ion recovery and low fluorinated by-product formation, and operate under relatively mild conditions with inexpensive reagents. The proposed mechanism is consistent with both computational and experimental results, provides insight into the complexity of PFAS mineralization processes, and may be operative but unrecognized in other PFAS degradation approaches. This demonstration of the reactivity of perfluoroalkyl anions, and the ability to access such intermediates efficiently from PFCAs, may inform the development of engineered PFAS degradation processes and facilitate expanding this reactivity mode to PFAS with other polar head groups.

REFERENCES AND NOTES

1. A. Leeson *et al.*, *Environ. Toxicol. Chem.* **40**, 24–36 (2021).
2. A. M. Calafat, L.-Y. Wong, Z. Kuklenyik, J. A. Reidy, L. L. Needham, *Environ. Health Perspect.* **115**, 1596–1602 (2007).
3. United Nations Stockholm Convention, "Perfluorooctanoic acid (PFOA), its salts and PFOA-related compounds" (UN, 2017); http://chm.pops.int/Implementation/Alternatives/AlternativestoPOPs/ChemicalslistedinAnnexA/PFOA/tabid/8292/Default.aspx.
4. "C-8 Medical Monitoring Program" (GCG, 2022); http://www.c-8medicalmonitoringprogram.com/.
5. N. Rich, "Rob Bilott v. DuPont," *New York Times Magazine*, 17 January 2016; https://hnbpjs.blogspot.com/2016/01/rob-bilott-v-dupont.html.
6. A. Maimaiti *et al.*, *Chem. Eng. J.* **348**, 494–502 (2018).
7. M. Ateia, A. Alsbaiee, T. Karanfil, W. Dichtel, *Environ. Sci. Technol. Lett.* **6**, 688–695 (2019).
8. D. Bond, J. Enck, "First in the nation testing reveals toxic contamination in soil and water near Norlite incinerator" (Bennington University, 2020); https://www.bennington.edu/sites/default/files/sources/docs/Norlite%20News%20Release%20%5Bdb%20final%20updated%5D.pdf.
9. C. D. Vecitis, H. Park, J. Cheng, B. T. Mader, M. R. Hoffmann, *J. Phys. Chem. A* **112**, 4261–4270 (2008).
10. J. Cheng, C. D. Vecitis, H. Park, B. T. Mader, M. R. Hoffmann, *Environ. Sci. Technol.* **44**, 445–450 (2010).
11. R. K. Singh *et al.*, *Environ. Sci. Technol.* **53**, 2731–2738 (2019).
12. C. E. Schaefer, C. Andaya, A. Urtiaga, E. R. McKenzie, C. P. Higgins, *J. Hazard. Mater.* **295**, 170–175 (2015).
13. A. M. Trautmann, H. Schell, K. R. Schmidt, K. M. Mangold, A. Tiehm, *Water Sci. Technol.* **71**, 1569–1575 (2015).
14. M. J. Krause *et al.*, *J. Environ. Eng.* **148**, 05021006 (2022).
15. M. J. Bentel *et al.*, *Environ. Sci. Technol. Lett.* **7**, 351–357 (2020).
16. M. J. Bentel *et al.*, *Environ. Sci. Technol.* **53**, 3718–3728 (2019).
17. M. J. Bentel *et al.*, *Environ. Sci. Technol.* **54**, 2489–2499 (2020).
18. H. Hori *et al.*, *Environ. Sci. Technol.* **39**, 2383–2388 (2005).
19. X. Liang, J. Cheng, C. Yang, S. Yang, *Chem. Eng. J.* **298**, 291–299 (2016).
20. B. N. Nzeribe, M. Crimi, S. Mededovic Thagard, T. M. Holsen, *Crit. Rev. Environ. Sci. Technol.* **49**, 866–915 (2019).
21. Q. Zhuo, S. Deng, B. Yang, J. Huang, G. Yu, *Environ. Sci. Technol.* **45**, 2973–2979 (2011).
22. H. Hori *et al.*, *Environ. Sci. Technol.* **38**, 6118–6124 (2004).
23. B. Wu *et al.*, *Environ. Sci. Technol. Lett.* **6**, 630–636 (2019).
24. D. Kong, P. J. Moon, E. K. J. Lui, O. Bsharat, R. J. Lundgren, *Science* **369**, 557–561 (2020).
25. S. Zhou, B. T. Nguyen, J. P. Richard, R. Kluger, J. Gao, *J. Am. Chem. Soc.* **143**, 137–141 (2021).
26. H. K. Liberatore, S. R. Jackson, M. J. Strynar, J. P. McCord, *Environ. Sci. Technol. Lett.* **7**, 477–481 (2020).
27. C. Zhang, A. C. McElroy, H. K. Liberatore, N. L. M. Alexander, D. R. U. Knappe, *Environ. Sci. Technol.* **56**, 6103–6112 (2022).
28. D. A. Dixon, T. Fukunaga, B. E. Smart, *J. Am. Chem. Soc.* **108**, 4027–4031 (1986).
29. T. Chatterjee, E. Boutin, M. Robert, *Dalton Trans.* **49**, 4257–4265 (2020).
30. J. D. LaZerte, L. J. Hals, T. S. Reid, G. H. Smith, *J. Am. Chem. Soc.* **75**, 4525–4528 (1953).
31. R. N. Haszeldine, *J. Chem. Soc.*4259 (1952).
32. X. Zhang, U. Gross, K. Seppelt, *Angew. Chem. Int. Ed.* **34**, 1858–1860 (1995).
33. M. J. Pellerite, *J. Fluor. Chem.* **49**, 43–66 (1990).
34. Y. Ge *et al.*, *Comput. Theor. Chem.* **1029**, 33–40 (2014).
35. G. McGrath, "Denied by Trump EPA, NC activists hope Biden EPA will force 'forever chemical' study," *Fayetteville Observer*, 17 January 2021; https://www.fayobserver.com/story/news/2021/01/27/denied-by-trump-epa-nc-activists-hope-biden-epa-force-forever-chemical-study/4265453001/.

ACKNOWLEDGMENTS

We thank Y. Luo at Shanghai Institute of Organic Chemistry for helpful discussions about fluorine NMR; S. Shafaie at Northwestern University's Integrated Molecular Structure Education and Research Center (IMSERC) facility for assistance with MS; and R. Sponenburg at Northwestern University's Quantitative Bio-element Imaging Center (QBIC) for ion chromatography.
Funding: B.B.T. is supported by the National Science Foundation Graduate Research Fellowship Program (NSF grant DGE-1842165). K.N.H. is supported by the National Science Foundation (grant CHE-1764328) and the Saul Winstein Chair in Organic Chemistry. Ion chromatography was performed at the Northwestern University Quantitative Bio-element Imaging Center, which is generously supported by the NASA Ames Research Center (grant NNA04CC36G). This work made use of the IMSERC at Northwestern University, which has received support from the National Institutes of Health (NIH grants 1S10OD012016-01 and 1S10RR019071-01A1), the Soft and Hybrid Nanotechnology Experimental (SHyNE) Resource

(NSF grant ECCS-1542205), the State of Illinois, and the International Institute for Nanotechnology (IIN). Gas chromatography MS was performed at the REACT Core Facility at Northwestern University, which acknowledges funding from the U.S. Department of Energy, Office of Science, Office of Basic Energy Sciences, Catalysis Science program (DE-SC0001329) used for the purchase of the GC/MS analysis system. **Author contributions:** Conceptualization: B.B.T., K.N.H., W.R.D.; Data curation: L.Y.L.; Formal analysis: B.B.T., L.Y.L., M.A.; Funding acquisition: K.N.H., W.R.D.; Investigation: B.B.T., L.Y.L.; Methodology: B.B.T., L.Y.L., K.N.H., W.R.D.; Project administration: K.N.H., W.R.D.; Supervision: X.S.X., K.N.H., W.R.D.; Visualization: B.B.T., L.Y.L.; Writing – original draft: B.B.T., L.Y.L., K.N.H., W.R.D.; Writing – review & editing: B.B.T., L.Y.L., X.S.X., M.A., K.N.H., W.R.D. **Competing interests:** Northwestern University has filed a provisional patent (63/261,772) that describes methods to degrade PFCAs on behalf of inventors B.B.T. and W.R.D. W.R.D. is a founder and equity holder in Cyclopure, Inc., which is commercializing technologies related to PFAS detection and remediation. Cyclopure is uninvolved in the research described in this manuscript. The remaining authors declare no competing interests. **Data and materials availability:** All data are available in the manuscript or the supplementary materials. **License information:** Copyright © 2022 the authors, some rights reserved; exclusive licensee American Association for the Advancement of Science. No claim to original US government works. https://www.science.org/about/science-licenses-journal-article-reuse

SUPPLEMENTARY MATERIALS

science.org/doi/10.1126/science.abm8868
Materials and Methods
Supplementary Text
Figs. S1 to S66
Tables S1 to S4
Data S1
References (*36*–*57*)

Submitted 19 October 2021; resubmitted 19 April 2022
Accepted 8 July 2022
10.1126/science.abm8868

Science

Low-temperature mineralization of perfluorocarboxylic acids

Brittany TrangYuli LiXiao-Song XueMohamed AteiaK. N. HoukWilliam R. Dichtel

Science, 377 (6608), • DOI: 10.1126/science.abm8868

Forever chemicals' Achilles' heel

Per- and polyfluoroalkyl substances (PFAS) have been referred to as "forever chemicals" because of their resistance to most biological and chemical degradation mechanisms. Most current methods use very harsh conditions to decompose these compounds. Trang *et al*. found that there is a potential weak spot in carboxylic acid–containing PFAS: Decarboxylation in polar, non-protic solvents yields a carbanion that rapidly decomposes (see the Perspective by Joudan and Lundgren). The authors used computational work and experiments to show that this process involves fluoride elimination, hydroxide addition, and carbon–carbon bond scission. The initial decarboxylation step is rate limiting, and subsequent defluorination and chain shortening steps occur through a series of low barrier steps. The procedure can accommodate perfluoroether carboxylic acids, although sulfonic acids are not currently compatible. — MAF

View the article online
https://www.science.org/doi/10.1126/science.abm8868
Permissions
https://www.science.org/help/reprints-and-permissions

Use of this article is subject to the Terms of service

Science (ISSN) is published by the American Association for the Advancement of Science. 1200 New York Avenue NW, Washington, DC 20005. The title *Science* is a registered trademark of AAAS.
Copyright © 2022 The Authors, some rights reserved; exclusive licensee American Association for the Advancement of Science. No claim to original U.S. Government Works